J Math Chem (2012) 50:1289–1303
DOI 10.1007/s10910-011-9970-9

ORIGINAL PAPER

General formulae for interacting spherical nanoparticles and fullerenes

Richard K. F. Lee · James M. Hill

Received: 21 October 2011 / Accepted: 28 December 2011 / Published online: 7 January 2012

Abstract Most nanodevices under investigation adopt a computational approach such as molecular dynamics simulations, which gives a numerical value for the potential energy as calculated from the interaction of every atom on one molecule with every atom on a second molecule. Although the simulation only involves short range atom–atom interactions and ignores those interactions at longer distances, the simulation still involves significant computational time. In this paper, we determine analytical formulae for four types of Lennard–Jones interactions: (i) a solid spherical nanoparticle with an atom, (ii) two distinct radii hollow spherical fullerenes, (iii) a solid spherical nanoparticle with a hollow spherical fullerene and (iv) two distinct radii solid spherical nanoparticles. The interaction energy using the 6–12 Lennard–Jones potential for these four situations are determined using the continuum approximation, which assumes that a discrete atomic structure can be replaced by either an average atomic surface density or an average atomic volume density. Using these formulae the computational time for a simulation might be dramatically reduced for those molecular interactions involving spherical nanoparticles or fullerenes. Such formulae might be exploited in hybrid analytical-computational numerical schemes, as well as in metallofullerenes and certain assumed spherical models of molecules such as methane and ammonia. As an illustration of the formulae presented here we determine both the most stable and the maximum radii of a solid spherical nanoparticle inside a fullerene, modelling the centre of a carbon onion or metallofullerenes. We also determine new

R. K. F. Lee (✉) · J. M. Hill
Nanomechanics Group, School of Mathematical Sciences, The University of Adelaide, Adelaide, SA 5005, Australia
e-mail: Dr.rkf.lee@gmail.com

J. M. Hill
e-mail: jim.hill@adelaide.edu.au

cut-off formulae for interacting spherical nanoparticles and fullerenes which might be useful in computational schemes.

Keywords Sphere · Fullerenes · Nanoparticle · Lennard–Jones potential · Nanoparticle · Molecular dynamics simulations

1 Introduction

Nowadays, nanotechnology impinges on every aspect of our lives. For example, every time we touch a computer keyboard, a telephone or any device which needs to resist bacterial growth, we are infact touching silver nanoparticles [1,2]. Nanomaterials include, for example, fullerenes, nanotubes, nanowires, nanoparticles and nanoribbons, which are involved in many areas of application, such as gas separation [3] and storage [4], oscillators [5,6], medicine [7] and memory devices [8,9].

Most nanodevices contain nanotubes, fullerenes and nanoparticles as components, such as gold nanoparticles and multiwall carbon nanotubes [10], nanoparticles inside nanotubes [11,12], nanoparticles in liquids [13], nanoparticles in polymers [14] and fullerenes inside nanotubes for nanocomputing [15]. Generally, to study these systems [13–15] a molecular dynamics simulation is used which calculates the potential energy for each atom–atom interaction and accordingly requires considerable computational time. Molecular dynamics simulation is a numerical method that only takes into account the short range Lennard–Jones interactions, and the longer range interactions are assumed to be zero in order to reduce the computational time [13,14]. The potential energy is ignored when the distance between two atoms is greater than a certain cut-off distance $r_c = 2.5\sigma$ where σ is the van der Waals diameter. Cox et al. [16,17] have proposed using the Lennard–Jones potential for a spherical fullerene interacting with an atom. The formulae derived here could be exploited in conjunction with certain molecular dynamics simulations in order to reduce the computational time for those simulations involving spherical nanoparticles and fullerenes.

The formula for the Lennard–Jones interaction of an atom with a fullerene is well known (see for example Cox et al. [16,17]). In this study, we determine explicit formulae for the Lennard–Jones potentials for (i) a solid spherical nanoparticle with an atom, (ii) two distinct radii hollow spherical fullerenes, (iii) a solid spherical nanoparticle with a hollow spherical fullerene and (iv) two distinct radii solid spherical nanoparticles. Such formulae could reduce the computational time of a molecular dynamics simulation for those systems involving spherical nanoparticles and fullerenes. For example, most of molecular dynamics simulations use a super computer to evaluate the interaction energy of several spherical nanoparticles which involves a significant computational time. The formula presented here might significantly reduce this time. These formulae might also be adopted for metallofullerenes which are fullerenes with centrally located metal atoms, and represented by the notation $M@C_n$ where the symbol M is used to denote the additional atom inside the fullerene, and n indicates the total number of carbon atoms in the cage. The size of the metallofullerene is based on the number of carbon atoms n which ranges from 60 to 100 with the most stable abundant types being the $M@C_{80}$ and $M@C_{100}$ endohedral fullerenes [18]. In addition, the

same formulae could be used for certain models of molecules such as methane (CH_4) and ammonia (NH_3) which assume a central atom surrounded by a spherical surface of a certain radius and with the like atoms assumed to be uniformly distributed. Such models dramatically improve the computational efficiency [19,20].

In the following section, we introduce the 6–12 Lennard–Jones potential function for perfect solid spherical nanoparticles interacting with an atom and adopting the continuum approximation, which assumes that a discrete atomic structure can be approximated by an average constant atomic surface or volume density. The 6–12 Lennard–Jones potential energy formulae for two distinct radii spheres; a fullerene with a fullerene; a nanoparticle with a fullerene and a nanoparticle with a nanoparticle are presented in Sects. 3, 4 and 5, respectively. New formulae for cut-off distances are discussed in Sect. 6 and an application modelling carbon onion centres and metallofullerenes is discussed in Sect. 7. Finally, some overall concluding remarks are made in Sect. 8.

2 Nanoparticle with atom

The Lennard–Jones potential is used for two non-bonded molecular structures and the classical 6–12 Lennard–Jones potential for two atoms at a distance r apart is given by $\Phi(r) = -(A/r^6) + (B/r^{12})$, where A and B denote the attractive and the repulsive constants, respectively [21]. This equation can also be rewritten as $\Phi(r) = 4\epsilon[-(\sigma/r)^6 + (\sigma/r)^{12}]$, where $r_0 = 2^{1/6}\sigma = (2B/A)^{1/6}$ is the equilibrium distance, σ is the van der Waals diameter and $\epsilon = A^2/(4B)$ is the well depth [21]. The van der Waals diameter σ_{ab} and the well depth ϵ_{ab} for two different materials, say materials a and b, can be found from the arithmetic mean $\sigma_{ab} = (\sigma_a + \sigma_b)/2$ and the geometric mean $\epsilon_{ab} = (\epsilon_a\epsilon_b)^{1/2}$ where the labels a, b and ab refer to the interactions between a material, b material and ab materials, respectively [21], and the numerical values used for the 6-12 Lennard–Jones constants are as shown in Table 2.

The total interaction energy for two non-bonded molecules is obtained by summation of the interaction energy for each non-bonded atomic pair, thus $E = \sum_i \sum_j \Phi(r_{ij})$, where $\Phi(r_{ij})$ is the interaction potential energy for non-bonded atoms i and j at a distance r_{ij} apart. The continuum approximation assumes that the total interaction energy can be approximated by a double surface integral, a surface-volume integral or a double volume integral. The double surface integral is used for two hollow molecules such as fullerene–fullerene interactions, $E = \eta_1\eta_2 \int_{S_2}\int_{S_1} \Phi(r)dS_1dS_2$, where η_1 and η_2 denote the mean atomic surface densities of each molecule and r denotes the distance between two typical surface elements dS_1 and dS_2. The surface-volume integral is used for a hollow molecule with a solid molecule such as fullerene-nanoparticle interactions, $E = \eta\rho \int_V \int_S \Phi(r)dSdV$, where η denotes the mean atomic surface density of molecule, ρ denotes the average atomic density of molecule and r denotes the distance between two typical elements dS and dV. The double volume integral is used for two solid molecules such as nanoparticle–nanoparticle interactions, $E = \rho_1\rho_2 \int_{V_2}\int_{V_1} \Phi(r)dV_1dV_2$, where ρ_1 and ρ_2 denote the mean atomic densities of each molecule and r denotes the distance between two typical volume elements dV_1 and dV_2.

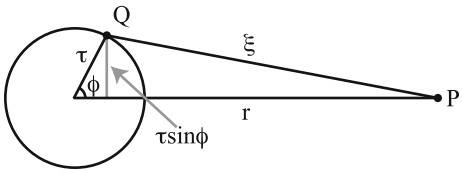

Fig. 1 Geometry for solid spherical nanoparticle interacting with an atom

Figure 1 shows the geometry of a perfect spherical nanoparticle which is interacting with an atom. The total interaction energy for a perfect spherical nanoparticle with an atom is determined by the volume integral,

$$E_p(r) = \rho \int_V \left(-\frac{A}{\xi^6} + \frac{B}{\xi^{12}} \right) dV,$$

where ρ is the average atomic density for the nanoparticle, namely number of atoms per unit volume, and ξ is the distance between the atoms at the points P and Q given by $\xi^2 = r^2 + \tau^2 - 2r\tau\cos\phi$. At the point Q, we generate a ring of radius $\tau\sin\phi$, we find that the potential energy for an atom interacting with all atoms of the sphere of radius a is given by $E_p(r) = -P_6(r) + P_{12}(r)$ where $P_n(r)$ is defined by

$$\begin{aligned} P_n(r) &= C_n\rho \int_V \frac{1}{\xi^n} dV = C_n\rho \int_0^a \int_0^\pi \frac{2\pi\tau\sin\phi}{\xi^n} \tau d\phi d\tau \\ &= \frac{2C_n\rho\pi}{r(n-2)} \left[-\frac{1}{(n-4)(r+a)^{n-4}} + \frac{r}{(n-3)(r+a)^{n-3}} \right. \\ &\quad \left. -\frac{1}{(n-4)(r-a)^{n-4}} + \frac{r}{(n-3)(r-a)^{n-3}} + \frac{2}{(n-3)(n-4)r^{n-4}} \right], \end{aligned} \tag{1}$$

where the coefficients $C_6 = A$ and $C_{12} = B$, and r is the distance between the atom and the centre of the spherical nanoparticle.

Equations such as (1) might be exploited for those molecular dynamics simulations comprising solid spherical nanoparticles which are interacting with other more complicated molecules and the computational time might be considerably reduced.

3 Fullerene with fullerene

The interaction between two distinct radii spherical fullerenes can be considered as the interaction of two different sized hollow spheres, as illustrated in Fig. 2. In a molecular dynamics simulation, the total interaction energy for two fullerenes is determined as the sum of the interactions for each atom on the left sphere with each atom on the right sphere. However, using the continuum approach, the interaction energy is determined from the double surface integral, $E = \eta_1\eta_2 \int_{S_2} \int_{S_1} \Phi(r) dS_1 dS_2$.

The first surface integral is the interaction energy of a fullerene with an atom, as illustrated in Fig. 2 with the single atom interacting with the right sphere. The energy

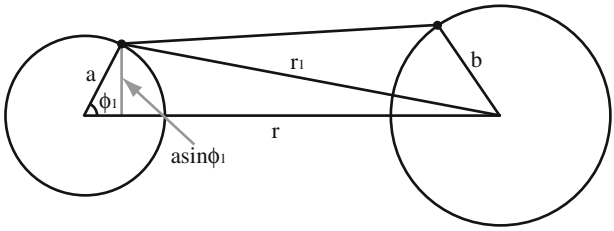

Fig. 2 Geometry for two fullerenes

$E_f(r)$ for a spherical fullerene interacting with one atom is as derived in Cox et al. [16] and is given by

$$E_f(r) = \frac{\eta_{f1}\pi b}{r}\left\{\frac{A}{2}\left[\frac{1}{(r+b)^4}-\frac{1}{(r-b)^4}\right]-\frac{B}{5}\left[\frac{1}{(r+b)^{10}}-\frac{1}{(r-b)^{10}}\right]\right\}, \quad (2)$$

where b is the radius for the fullerene and η_{f1} is the mean atomic surface density of the fullerene. The energy for the fullerene with an atom (Eq. 2) may be rewritten as $E = -Q_6 + Q_{12}$ where

$$Q_n(r_1) = \frac{2C_n\eta_{f1}\pi b}{r_1(2-n)}\left\{\frac{1}{(r_1+b)^{n-2}} - \frac{1}{(r_1-b)^{n-2}}\right\}, \quad (3)$$

and the constants C_6 and C_{12} are the Lennard–Jones constants A and B, respectively.

Figure 2 shows that the distance of any atom on the left fullerene from the centre of the right fullerene is $r_1^2 = a^2 + r^2 - 2ar\cos\phi_1$, where a is the radius of the left fullerene. For the second surface integral based on Eq. (3), the energy for two distinct radii fullerenes becomes $E_{f-f}(r) = -G_6(r) + G_{12}(r)$ where G_n is given by

$$\begin{aligned} G_n(r) &= \eta_{f2}\int_{S2} Q_n dS_2 = 2\pi\eta_{f2}\int_0^{\pi} Q_n a^2 \sin\phi_1 d\phi_1 \\ &= \frac{4C_n\pi^2\eta_{f1}\eta_{f2}ab}{r(n-2)(n-3)}\left[\frac{1}{(r+a+b)^{n-3}} - \frac{1}{(r-a+b)^{n-3}}\right. \\ &\quad \left. -\frac{1}{(r+a-b)^{n-3}} + \frac{1}{(r-a-b)^{n-3}}\right], \end{aligned} \quad (4)$$

where $C_6 = A$, $C_{12} = B$ and η_{f2} is the mean atomic surface density for the second fullerene.

4 Nanoparticle with fullerene

Nano-systems may involve spherical nanoparticles and spherical fullerenes, and therefore the 6–12 Lennard–Jones potential for a nanoparticle with a fullerene is introduced in this section. The potential energy of a nanoparticle with a fullerene is found from the surface-volume integral which is used for a hollow molecule with a solid molecule,

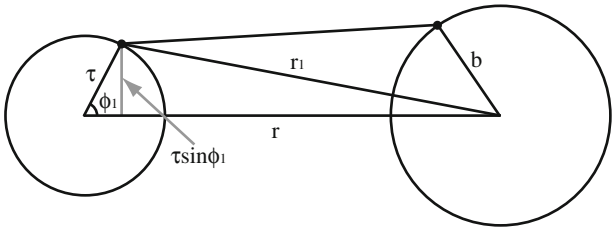

Fig. 3 Geometry for two spheres

$E = \eta\rho \int_V \int_S \Phi(r) dS dV$, where η denotes the mean atomic surface density of the molecule, ρ denotes the average atomic volume density of the molecule and r denotes the distance between two typical elements dS and dV.

The surface integral is the potential energy for a fullerene with an atom, Eq. (2). As a result, the Lennard–Jones potential for a nanoparticle with a fullerene is the volume integral obtained from Eq. (3).

Figure 3 shows that the distance of any atom on the left sphere with the centre of the right sphere is $r_1^2 = \tau^2 + r^2 - 2\tau r \cos\phi_1$, where τ is the radius of any atom on left sphere and the radius of the left sphere is a. For the volume integral, the energy for the solid sphere and the hollow sphere with two distinct radii is found as $E_{f-p}(r) = -H_6(r) + H_{12}(r)$ where H_n is given by

$$
\begin{aligned}
H_n &= \rho \int_V Q_n dV = 2\pi\rho \int_0^a \int_0^\pi Q_n \tau^2 \sin\phi_1 d\phi_1 d\tau \\
&= \frac{4C_n\pi^2\rho\eta b}{r(n-2)(n-3)} \left[-\frac{1}{(n-5)(r+a+b)^{n-5}} + \frac{r+b}{(n-4)(r+a+b)^{n-4}} \right. \\
&\quad + \frac{1}{(n-5)(r-a+b)^{n-5}} - \frac{r+b}{(n-4)(r-a+b)^{n-4}} \\
&\quad + \frac{1}{(n-5)(r+a-b)^{n-5}} - \frac{r-b}{(n-4)(r+a-b)^{n-4}} \\
&\quad \left. - \frac{1}{(n-5)(r-a-b)^{n-5}} + \frac{r-b}{(n-4)(r-a-b)^{n-4}} \right],
\end{aligned} \tag{5}
$$

where ρ is the mean atomic volume density and η is the mean atomic surface density.

5 Nanoparticle with nanoparticle

The Lennard–Jones potential for two distinct radii spherical nanoparticles will be presented in this section. The potential energy is found by a double volume integral, $E = \rho_1\rho_2 \int_{V_2} \int_{V_1} \Phi(r) dV_1 dV_2$, where ρ_1 and ρ_2 denote the average atomic volume densities of molecules, 1 and 2, respectively and r denotes the distance between two typical volume elements dV_1 and dV_2.

Similarly, the first volume integral is the potential energy for a nanoparticle with an atom therefore the equation for the first volume integral is found from Sect. 2,

$E_p = -P_6 + P_{12}$, where P_n is Eq. (1). For the second volume integral, the potential energy equation is found as $E_{p-p} = -I_6 + I_{12}$ where I_n is given by

$$
\begin{aligned}
I_n &= \rho_2 \int_2 P_n dV_2 = 2\pi\rho_2 \int_0^a \int_0^\pi P_n \tau^2 \sin\phi_1 d\phi_1 d\tau \\
&= \frac{4C_n\pi^2\rho_1\rho_2}{(n-2)(n-3)(n-4)} \int_0^a \Bigg[\frac{1}{(n-5)(r+\tau+b)^{n-6}} \\
&\quad + \frac{-r+(n-6)b}{(n-5)(r+\tau+b)^{n-5}} - \frac{b(r+b)}{(r+\tau+b)^{n-4}} + \frac{1}{(n-5)(r+\tau-b)^{n-6}} \\
&\quad - \frac{r+(n-6)b}{(n-5)(r+\tau-b)^{n-5}} + \frac{b(r-b)}{(r+\tau-b)^{n-4}} - \frac{2}{(n-5)(r+\tau)^{n-6}} \\
&\quad + \frac{2r}{(n-5)(r+\tau)^{n-5}} + \frac{1}{(n-5)(r-\tau+b)^{n-6}} + \frac{-r+(n-6)b}{(n-5)(r-\tau+b)^{n-5}} \\
&\quad - \frac{b(r+b)}{(r-\tau+b)^{n-4}} + \frac{1}{(n-5)(r-\tau-b)^{n-6}} - \frac{r+(n-6)b}{(n-5)(r-\tau-b)^{n-5}} \\
&\quad + \frac{b(r-b)}{(r-\tau-b)^{n-4}} - \frac{2}{(n-5)(r-\tau)^{n-6}} + \frac{2r}{(n-5)(r-\tau)^{n-5}} \Bigg] d\tau,
\end{aligned}
$$

where ρ_1 and ρ_2 are the average atomic volume densities. However at the moment, the value of n could be 6 and therefore some terms of the integral become $\int 1/x dx$. As a result, I_6 becomes

$$
\begin{aligned}
I_6 = \frac{A\pi^2\rho_1\rho_2}{6} \Bigg[& r \ln\left(\frac{(r-a)^2-b^2}{(r+a)^2-b^2}\right) + 2r \ln\left(\frac{r+a}{r-a}\right) + \frac{b(r+b)}{(r+a+b)} \\
& - \frac{b(r-b)}{(r+a-b)} - \frac{b(r+b)}{(r-a+b)} + \frac{b(r-b)}{(r-a-b)} \Bigg],
\end{aligned}
$$

and for n greater than 6, I_n is found to be

$$
\begin{aligned}
I_n = \frac{4C_n\pi^2\rho_1\rho_2}{(n-2)(n-3)(n-4)(n-5)} \Bigg[& - \frac{r+(n-6)a+(n-6)^2b}{(n-6)(n-7)(r+a+b)^{n-6}} \\
& + \frac{b(r+b)}{(r+a+b)^{n-5}} - \frac{r+(n-6)a-(n-6)^2b}{(n-6)(n-7)(r+a-b)^{n-6}} - \frac{b(r-b)}{(r+a-b)^{n-5}} \\
& + \frac{2(r+(n-6)a)}{(n-6)(n-7)(r+a)^{n-6}} + \frac{r-(n-6)a+(n-6)^2b}{(n-6)(n-7)(r-a+b)^{n-6}} \\
& - \frac{b(r+b)}{(r-a+b)^{n-5}} + \frac{r-(n-6)a-(n-6)^2b}{(n-6)(n-7)(r-a-b)^{n-6}} + \frac{b(r-b)}{(r-a-b)^{n-5}} \\
& - \frac{2(r-(n-6)a)}{(n-6)(n-7)(r-a)^{n-6}} \Bigg].
\end{aligned}
$$

Table 1 Parameters of fullerenes C_n [22]

Fullerene	Radius (Å)	η (Å^{-2})
C_{60}	3.55	0.37887
C_{82}	4.15	0.37889
C_{240}	7.06	0.38317
C_{540}	10.53	0.38755
C_{960}	14.02	0.38866
C_{1500}	17.5225	0.38877
C_{2160}	20.95	0.39163
C_{2940}	23.8728	0.41052
C_{3840}	27.95	0.39116

6 Summary and discussion

For each of the Lennard–Jones potential formulae derived here involving spheres along with the Lennard–Jones atom–atom parameters, they also require two more parameters for each formula which are the radius of the sphere and the mean atomic surface density for a hollow sphere or the mean atomic volume density for a solid sphere. Table 1 shows the parameter values for the radii and the mean atomic surface densities for spherical fullerenes. For the nanoparticle parameters, the radius of the carbon nanoparticle have a large range from 1.5 nm [23] to 30 nm [24]. The density of the amorphous carbon nanoparticles is similar to the amorphous carbon density 2.2670 g cm^{-3} [23], therefore the mean atomic volume density is 0.11366 Å^{-3} for the carbon nanoparticles and used in Figs. 4a, c, 5b, d and 6.

Figure 4 shows the interaction energy for a carbon atom with (a) a carbon nanoparticle and (b) a carbon C_{60} fullerene for which both radii are 3.55 Å. The minimum energy for a fullerene with an atom is deeper than that for a nanoparticle with one atom. Similarly, the location of the minimum energy for the fullerene-atom is greater than that for the nanoparticle-atom. This phenomena is a consequence of the total number of atoms of the nanoparticle in question. The total number of atoms of the nanoparticle and the fullerene are 21 and 60, respectively and therefore the attractive energy for the nanoparticle-atom must be less than that for the fullerene-atom. The distance of the minimum energy location for the fullerene-atom is greater than that for the nanoparticle-atom, because the fullerene has more atoms on the spherical surface and therefore gives the minimum energy location at a longer distance.

In order to save computational time, numerical simulations only count atomic interactions inside a cut-off distance $r_c = 2.5\sigma$, where σ is the van der Waals diameter. The cut-off distance for the interaction of a solid or hollow sphere with an atom is found to be $r_c = 2.5(\sigma + d)$, where d is either a or b as the radius of the nanoparticle or fullerene, respectively. Figure 4 shows the interaction energy for (c) the nanoparticle-atom and (d) the fullerene-atom at the cut-off distance for spheres of radius varying from 1 to 100 Å. The simulation ignores the interaction energy for any nanoparticle-atom or any fullerene-atom at locations which exceed the cut-off distance, so that the simulation has a cumulation error from the ignored energy, and therefore the maximum

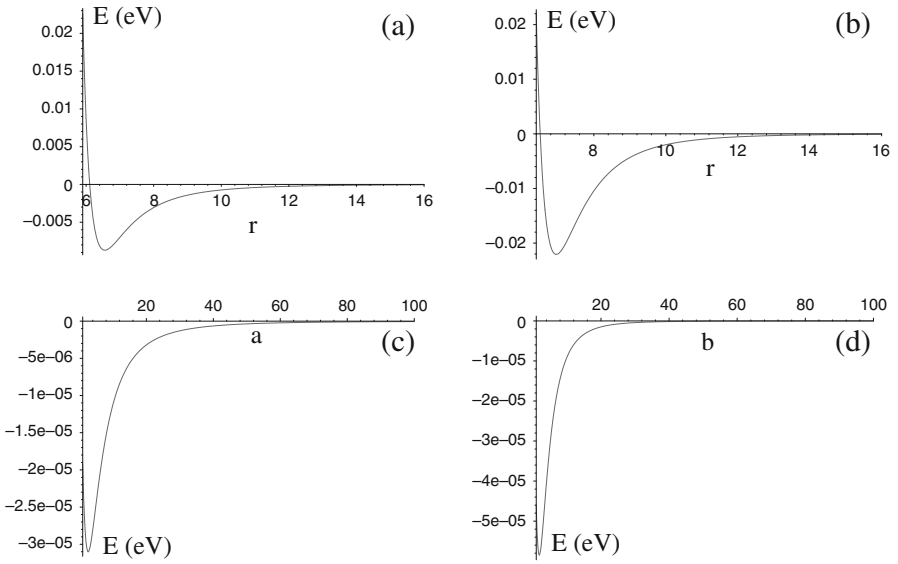

Fig. 4 Interaction energy for **a** carbon nanoparticle with carbon atom ($a = 3.55$ Å, $\rho = 0.11366$, r = 5.9 to 16 Å) **b** carbon fullerene with carbon atom ($b = 3.55$ Å, $\eta = 0.37887$, r = 6.4 to 16 Å); Interaction energy at cut-off distance for **c** carbon nanoparticle with carbon atom ($a = 1$ to 100 Å, $\rho = 0.11366$) **d** carbon fullerene with carbon atom ($b = 1$ to 100 Å, $\eta = 0.37887$)

ignored energy is as small as possible. The ignored energy for the nanoparticle-atom is less than -0.000031 eV and for the fullerene-atom is less than -0.00006 eV which are the maximum ignored energies arising for sphere radii varying from 2 to 3Å, and it tends to zero for increasing sphere radius.

Adisa et al. [19] have compared the interaction energies of methane molecules in carbon nanotubes, modelling the CH_4 molecule as a spherical surface of a certain radius, with four smeared hydrogen atoms and with a carbon atom situated at the centre. The numerical results show that the average interaction for 100 different orientations of the methane molecule inside a carbon nanotube agree well with the modelling results. Such a modelling approach is an important idealization which might dramatically improve computational time. Some molecular dynamics simulations for methane storage [25–28] consider many methane molecules and metallofullerenes interacting with carbon nanotubes and these interactions have been successfully modelled by the present authors [29] using the aproach adopted in Ref. [19].

Figure 5 shows the interaction energy for (a) C_{60} and C_{240} fullerenes and (b) a 4 Å radius carbon nanoparticle with a C_{60} fullerene. Figure 5c and d shows the interaction energy at the cut-off distance for the radii a and b varying from 1 to 100Å. The cut-off distance for two distinct radii fullerenes and for two distinct radii fullerene and nanoparticle are $r_c = 2.5(\sigma + a + b)$ which includes both radii a and b. The maximum ignored energy for two distinct radii fullerenes is -0.00023 eV occurring at the radii $a = b = 3.8$ Å, and for two distinct radii fullerene and nanoparticle is -0.0001363 eV occurring at the radii $a = 11.25$ Å and $b = 7.6$ Å, and both ignored energies tend to zero for increasing sphere radii.

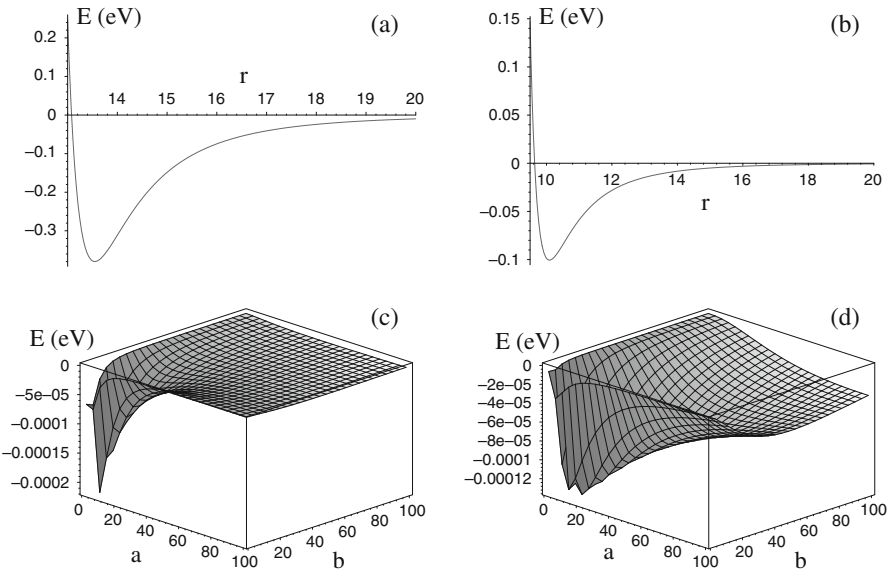

Fig. 5 Interaction energy for **a** carbon fullerene with carbon fullerene ($a = 7.06$ Å, b $= 3.55$ Å, $\eta_1 = 0.37887$, $\eta_2 = 0.38317$, r $=$ 13 to 20 Å) **b** carbon nanoparticle with carbon fullerene ($a = 4$ Å, b $= 3.55$ Å, $\rho = 0.11366$, $\eta = 0.37887$, $r = 9.5$ to 20 Å); Interaction energy at cut-off distance for **c** carbon fullerene with carbon fullerene ($a = 1$ to 100 Å), $b = 1$ to 100 Å, $\eta_1 = 0.37887$, $\eta_2 = 0.38317$) **d** carbon nanoparticle with carbon fullerene ($a = 1$ to 100 Å, $b = 1$ to 100 Å, $\rho = 0.11366$, $\eta = 0.37887$)

Figure 6a shows the interaction energy for two distinct radii nanoparticles and Fig. 6b, c show the interaction energy at the cut-off distance for radii a and b varying from 1 to 100 Å. For two distinct radii nanoparticles, the cut-off distance may have two values, one coincides with the above mentioned cut-off distance, namely $r_{c1} = 2.5(\sigma + a + b)$ and the other cut-off distance is $r_{c2} = 2.5\sigma + a^2/\sigma + b^2/\sigma$. Although the interaction energy at the $r_{c1} = 2.5(\sigma + a + b)$ cut-off distance does not tend to zero for increasing sphere radii, the ignored energy is around -0.3 eV for radii a and b equal to 100 Å, which is only 0.02% of the minimum energy. However, the first cut-off distance has a shorter interaction range and therefore has the advantage of reducing the computational time. For the second cut-off distance $r_{c2} = 2.5\sigma + a^2/\sigma + b^2/\sigma$, the maximum ignored energy is -0.23 eV occurring at radii a and b approximately equal to 5 Å and the ignored energy tends to zero for increasing sphere radii. The second cut-off distance has a longer interaction range due to a^2/σ and b^2/σ, and requires additional computational time. However, the second cut-off distance gives more accurate results for the energy.

7 Application

Endohedral fullerenes comprise atoms inside fullerenes, such as F^-, Ne, Na^+, Mg^{2+} or Al^{3+} [30]. Banhart and Ajayan [31] have reported diamond particles inside carbon onions, which comprise multi-walled nested fullerenes. If the additional atom is a

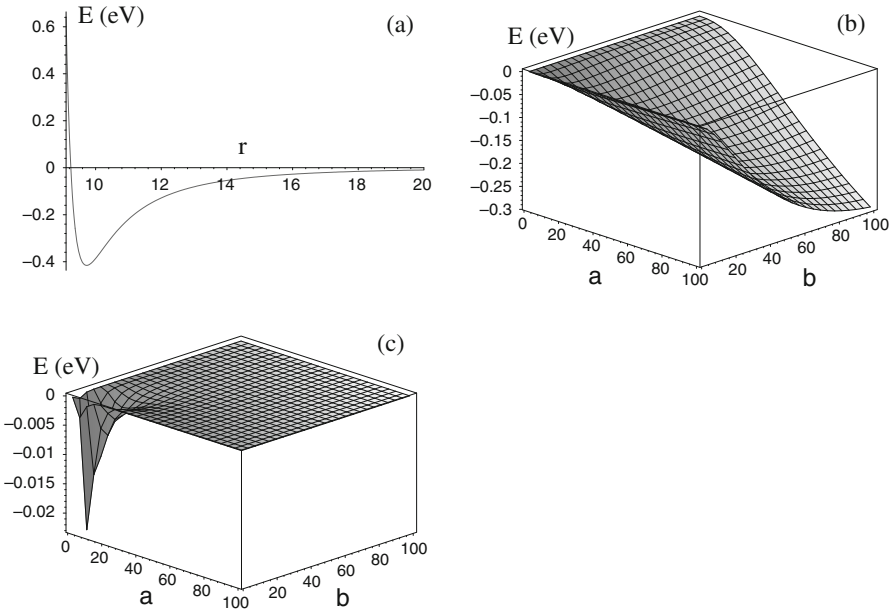

Fig. 6 **a** Interaction energy for carbon nanoparticle with carbon nanoparticle ($a = 4$ Å, b $= 3.55$ Å, $\rho_1 = \rho_2 = 0.11366$, $r = 9.1$ to 20 Å); **b** Interaction energy at cut-off distance $r_{c1} = 2.5(\sigma + a + b)$ for carbon nanoparticle with carbon nanoparticle ($a = 1$ to 100 Å, $b = 1$ to 100 Å, $\rho_1 = \rho_2 = 0.11366$); **c** Interaction energy at cut-off distance $r_{c2} = 2.5\sigma + a^2/\sigma + b^2/\sigma$ for carbon nanoparticle with carbon nanoparticle ($a = 1$ to 100 Å, $b = 1$ to 100 Å, $\rho_1 = \rho_2 = 0.11366$)

metal, then it is called an endohedral metallofullerene or simply a metallofullerene [32,33], and represented by the notation M@C_n where the symbol M is used to denote the additional atom inside the fullerene, and n indicates the total number of carbon atoms in the cage. The size of the endohedral fullerene is based on the number of carbon atoms n which ranges from 60 to 100 with the most stable abundant types being the M@C_{80} and M@C_{100} endohedral fullerenes [18]. M@C_{60} such as La@C_{60} and Ca@C_{60} metallofullerenes are unstable in air [18]. However, the most abundant neutral stable metallofullerenes are the M@C_n class ($n = 80, 82, 84$), such as Ca@C_{82}, Sc_3 N@C_{80}, Tb@C_{82}, Dy@C_{82}, La@C_{82}, Sc_2 @C_{84} [18].

We might utilise the interaction of a nanoparticle with a fullerene to determine the maximum possible size of a nanoparticle inside certain fullerenes. The interaction for the nanoparticle with the fullerene is found from $E_{f-p}(r) = -H_6(r) + H_{12}(r)$ where H_n is defined by Eq. (5). We assume that the nanoparticle is located at the centre of the fullerene, so that the distance r is zero and the energy $E_{f-p}(0)$ is found from the limit $r \to 0$ using L'Hôpital's rule and is given by

$$E_{f-p}(0) = -\frac{2A\pi^2\rho\eta b}{3}\left[\frac{3}{2(a+b)^2} - \frac{b}{(a+b)^3} - \frac{3}{2(a-b)^2} - \frac{b}{(a-b)^3}\right] + \frac{4B\pi^2\rho\eta b}{45}\left[\frac{9}{8(a+b)^8} - \frac{b}{(a+b)^9} - \frac{9}{8(a-b)^8} - \frac{b}{(a-b)^9}\right], \quad (6)$$

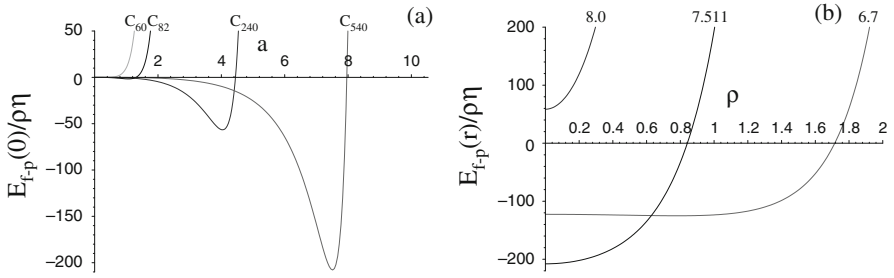

Fig. 7 **a** Energy $E_{f-p}(0)/(\rho\eta)$ for potassium nanoparticle at centre of C_{60}, C_{82}, C_{240} and C_{540} fullerenes and **b** Energy $E_{f-p}(r)/(\rho\eta)$ for potassium nanoparticle inside C_{540} fullerene with radius for 6.7, 7.511 and 8 Å

where A and B are the attractive and repulsive constants for a nanoparticle atom with a carbon atom.

The maximum permissible radius of a nanoparticle inside a fullerene is determined from the condition $E_{f-p}(0)/(\rho\eta) < 0$, where ρ and η are coefficients occurring in the energy. Figure 7a shows the energy $E_{f-p}(0)/(\rho\eta)$ for a potassium nanoparticle inside C_{60}, C_{82}, C_{240} and C_{540} fullerenes and shows the energy decreasing as the radius of the nanoparticle increases. However, the energy increases rapidly as the nanoparticle radius becomes close to the surface of the fullerene, since the distance between the two surfaces becomes small, and there is a greater repulsive contribution to the energy. When the energy $E_{f-p}(0)/(\rho\eta) > 0$, the additional atom cannot exist inside the fullerene since it would have a positive energy and therefore escape from the fullerene. As a result, the radius occurring at the minimum energy gives the radius of the most stable nanoparticle. If the radius of the nanoparticle is smaller than this radius, it will not locate at the centre of the fullerene because the minimum energy position will be offset from the centre of the fullerene. Figure 7b shows the energy $E_{f-p}(r)/(\rho\eta)$ for a potassium nanoparticle inside C_{540} with radii 6.7, 7.511 and 8 Å. For those nanoparticle radii between the most stable radius and the maximum radius, the endohedral fullerene is still stable. When the radius of the nanoparticle is greater than the maximum radius, the endohedral fullerene is not stable because the nanoparticle experiences a large repulsive force from the fullerene.

Tables 2 and 3 show that the numerical values of the 6–12 Lennard–Jones constants and the most stable and maximum radii for nanoparticles inside C_{60}, C_{82}, C_{240} and C_{540} fullerenes. In Tables 2 and 3 the star * indicates those materials which have no minimum energy while the hash # indicates that the energy $E_{f-p}(0)/(\rho\eta)$ is always greater than zero inside the C_{60} fullerene, and therefore these materials are unstable in the C_{60} fullerene, such as platinum, chlorine and iodine. For the other given numerical values of the Lennard–Jones constants for chlorine, the chlorine is predicted to be stable in the C_{60} fullerene.

8 Conclusion

Many nanodevices involve spherical nanoparticles or fullerenes as components, and they are usually investigated using a computational approach such as molecular

Table 2 6–12 Lennard–Jones constants and most stable radius of nanoparticle inside fullerene

	σ (Å)	$\lvert\epsilon\rvert$ (meV)	@C_{60} (Å)	@C_{82} (Å)	@C_{240} (Å)	@C_{540} (Å)
C_{60}–C_{60} [21]	3.47	2.86	*	*	*	*
K^+–K^+ [34]	3.564	3.0352	0.205	1.068	4.038	7.511
F^-–F^- [35]	2.224	0.403	1.072	1.693	4.615	8.086
Pt–Pt [36]	3.92	19.833	*	0.880	3.885	7.358
Zn–Zn [37]	2.462	5.372	0.956	1.587	4.513	7.984
Au–Au [38]	2.934	1.691	0.706	1.371	4.310	7.781
Mg^{2+}–Mg^{2+} [39]	0.7062	38.798	1.754	2.356	5.267	8.738
Mg^{2+}–Mg^{2+} [39]	0.8846	37.944	1.676	2.279	5.191	8.661
Mg^{2+}–Mg^{2+} [39]	0.9445	37.944	1.650	2.253	5.165	8.635
Cl^-–Cl^- [39]	2.156	4.336	1.104	1.724	4.645	8.115
Cl^-–Cl^- [40]	4.40	4.332	*	0.582	3.677	7.152
Cl^-–Cl^- [40]	4.05	6.509	*	0.806	3.828	7.302
Cl^-–Cl^- [40]	4.45	4.622	*	0.545	3.655	7.130
Na^+–Na^+ [40]	3.33	0.124	0.446	1.184	4.139	7.611
Na^+–Na^+ [40]	2.43	2.031	0.972	1.601	4.527	7.998
Na^+–Na^+ [40]	2.58	0.643	0.897	1.534	4.462	7.933
Li^+–Li^+ [41]	1.982	13.429	1.185	1.800	4.719	8.190
I^-–I^- [41]	3.819	10.149	*	0.935	3.928	7.401

* Indicates no most stable radius

dynamics simulation. This gives a numerical value for the potential energy as calculated from every atom–atom interaction, and due to the large number of atomic pairs in the system, the simulation may require considerable computational time. Many of these computational studies use the Lennard–Jones potential for the simulation of two non-bonded molecular structures. In this paper, we determine analytical formulae for the Lennard–Jones potential for the four interactions: (i) a solid spherical nanoparticle with an atom, (ii) a hollow spherical fullerene with another hollow spherical fullerene, (iii) a solid spherical nanoparticle with a hollow spherical fullerene and (iv) a solid spherical nanoparticle with another solid spherical nanoparticle. These formulae are based on the continuum approximation, which assumes that a discrete atomic structure can be replaced by an average atomic surface density or an average atomic volume density. The formulae presented here could be used to reduce the computational time in the determination of Lennard–Jones interactions for those systems involving spherical nanoparticles or spherical fullerenes.

Computational time is usually reduced by only considering short range atom–atom interactions, and ignoring those atomic interactions taking place over longer distances. Generally, the cut-off distance for atom–atom interactions is taken to be $r_c = 2.5\sigma$ where σ is the van der Waals diameter. However, the formulae presented here indicate that this is not suitable for those interactions involving spherical nanoparticles and fullerenes, and here the cut-off distance is found empirically from the derived

Table 3 Maximum radius of nanoparticle inside fullerene

	@C_{60} (Å)	@C_{82} (Å)	@C_{240} (Å)	@C_{540} (Å)
K^+–K^+ [34]	0.263	1.305	4.446	7.962
F^-–F^- [35]	1.290	1.964	4.967	8.462
Pt–Pt [36]	#	1.092	4.304	7.828
Zn–Zn [37]	1.164	1.857	4.876	8.374
Au–Au [38]	0.880	1.634	4.693	8.198
Mg^{2+}–Mg^{2+} [39]	1.977	2.597	5.540	9.021
Mg^{2+}–Mg^{2+} [39]	1.903	2.526	5.474	8.956
Mg^{2+}–Mg^{2+} [39]	1.878	2.502	5.451	8.934
Cl^-–Cl^- [39]	1.324	1.994	4.993	8.487
Cl^-–Cl^- [40]	#	0.737	4.111	7.646
Cl^-–Cl^- [40]	#	1.006	4.252	7.779
Cl^-–Cl^- [40]	#	0.691	4.090	7.627
Na^+–Na^+ [40]	0.567	1.433	4.538	8.050
Na^+–Na^+ [40]	1.181	1.872	4.888	8.386
Na^+–Na^+ [40]	1.098	1.803	4.831	8.330
Li^+–Li^+ [41]	1.411	2.070	5.060	8.552
I^-–I^- [41]	#	1.155	4.345	7.866

# Indicates no maximum radius

formulae to be $r_c = 2.5(\sigma + d)$ for the interaction of an atom with a solid or hollow sphere, where d is either a or b being the radius of the nanoparticle or the fullerene, respectively. For the interaction of a hollow or solid sphere with either a hollow or solid sphere, a reasanable cut-off distance is found to be $r_c = 2.5(\sigma + a + b)$, where a and b are two radii. For the interaction between two distinct radii solid spheres, the cut-off distance could be either $r_{c1} = 2.5(\sigma + a + b)$ or $r_{c2} = 2.5\sigma + a^2/\sigma + b^2/\sigma$. The former significantly reduces the computational time, while the latter provides a more accurate result for the energy.

As an illustration of the formulae presented here we determine both the most stable and the maximum radii of a solid spherical nanoparticle inside a fullerene, modelling the centre of a carbon onion or metallofullerenes. If the nanoparticle radius is less than the most stable value, then a stable equilibrium exists which may be offset from the centre of the fullerene. If the nanoparticle radius exceeds the maximum value, then the minimum energy location is unstable. For those nanoparticle radii between the most stable radius and the maximum radius, the nanoparticle is still stable. We determine these radii for certain materials such as K^+, F^-, Zn, Au, Mg^{2+}, Cl^-, Na^+ and Li^+ which are stable in a C_{60} fullerene.

Acknowledgments The support of the Australian Research Council through the Discovery Project Scheme is gratefully acknowledged.

References

1. A. Kumar, P.K. Vemula, P.M. Ajayan, G. John, Nat. Mater. **7**, 236–241 (2008)
2. R.M. Pattabi, K.R. Sridhar, S. Gopakumar, B. Vinayachandra, M. Pattabi, Int. J. Nanoparticles **3**(1), 53–64 (2010)
3. A.W. Thornton, T. Hilder, A.J. Hill, J.M. Hill, J. Membr. Sci. **336**, 101–108 (2009)
4. A.C. Dillon, K.M. Jones, T.A. Bekkedahl, C.H. Kiang, D.S. Bethune, M.J. Heben, Nature **386**, 377–379 (1997)
5. B.J. Cox, T.A. Hilder, D. Baowan, N. Thamwattana, J.M. Hill, Int. J. Nanotechnol. **5**(2/3), 195–217 (2003)
6. S.B. Legoas, V.R. Coluci, S.F. Braga, P.Z. Coura, S.O. Dantas, D.S. Galvão, Phys. Rev. Lett. **90**(5), 055504 (2003)
7. T.A. Hilder, J.M. Hill, Small **5**(3), 300–308 (2009)
8. R.K.F. Lee, J.M. Hill, CMC Comput. Mater. Continua. **20**(1), 85–100 (2010)
9. Y. Chan, R.K.F. Lee, J.M. Hill, IEEE Trans. Nanotechnol. **10**(5), 947–952 (2011)
10. B. Kim, W.M. Sigmund, Langmuir **20**, 8239–8242 (2004)
11. S. Arcidiacono, J.H. Walther, D. Poulikakos, D. Passerone, P. Koumoutsakos, Phys. Rev. Lett. **94**, 105502 (2005)
12. N.K. Zhevago, V.I. Glebov, Phys. Lett. A **250**, 360–368 (1998)
13. Y. Qin, K.A. Fichthorn, J. Chem. Phys. **119**(18), 9745–9754 (2003)
14. J.S. Smith, D. Bedrov, G.D. Smith, Compos. Sci. Technol. **63**, 1599–1605 (2003)
15. J.W. Kang, H.J. Hwang, Phys. E **23**, 36–44 (2004)
16. B.J. Cox, N. Thamwattana, J.M. Hill, Proc. R. Soc. A **463**, 461–476 (2007)
17. B.J. Cox, N. Thamwattana, J.M. Hill, Proc. R. Soc. A **463**, 477–494 (2007)
18. H. Shinohara, Rep. Prog. Phys. **63**, 843–892 (2000)
19. O.O. Adisa, B.J. Cox, J.M. Hill, Phys. B Condens. Matter **406**(1), 88–93 (2011)
20. O.O. Adisa, B.J. Cox, J.M. Hill, Micro. Nano Lett. **5**(5), 291–295 (2010)
21. L.A. Girifalco, M. Hodak, R.S. Lee, Phys. Rev. B **62**, 13104–13110 (2000)
22. D. Baowan, N. Thamwattana, J.M. Hill, Eur. Phys. J. D **44**, 117–123 (2007)
23. J.R. Hester, O.A. Louchev, Appl. Phys. Lett. **80**(14), 2580–2582 (2002)
24. A. Bezryadin, R.M. Westervelt, M. Tinkham, Appl. Phys. Lett. **74**(18), 2699–2701 (1999)
25. A.V. Vakhrushev, M.V. Suyetin, Nanotechnology **20**, 125602 (2009)
26. M.V. Suyetin, A.V. Vakhrushev, Nanoscale Res. Lett. **4**, 1267–1270 (2009)
27. E.I. Volkova, M.V. Suyetin, A.V. Vakhrushev, Nanoscale Res. Lett. **5**, 205–210 (2010)
28. M.V. Suyetin, A.V. Vakhrushev, Micro. Nano Lett. **4**(3), 172–176 (2009)
29. R.K.F. Lee, J.M. Hill, J. Nanosci. Nanotechnol. **11**(8), 6893–6903 (2011)
30. J. Cioslowski, E.D. Fleischmann, J. Chem. Phys. **94**(5), 3730–3734 (1991)
31. F. Banhart, P.M. Ajayan, Nature **382**, 433–435 (1996)
32. D.S. Bethune, R.D. Johnson, J.R. Salem, M.S. Vries, C.S. Yannoni, Nature **366**, 6451 (1993)
33. K. Laasonen, W. Andreoni, M. Parrinello, Science **258**, 1916–1918 (1992)
34. G. Chen, Y. Guo, N. Karasawa, W.A. Goddard III, Phys. Rev. B **48**(18), 13959 (1993)
35. H.J. Hwang, K.R. Byun, J.Y. Lee, J.W. Kang, Curr. Appl. Phys. **5**, 609–614 (2005)
36. T.A. Hilder, J.M. Hill, Micro. Nano Lett. **3**(1), 18–24 (2008)
37. R. Babarao, Z. Hu, J. Jiang, S. Chempath, S.I. Sandler, Langmuir **23**, 659–666 (2007)
38. Q. Pu, Y. Leng, X. Zhao, P.T. Cummings, Nanotechnology **18**, 424007 (2007)
39. K.M. Callahan, N.N. Casillas-Ituarte, M. Roeselová, H.C. Allen, D.J. Tobias, J. Phys. Chem. A **114**, 5141–5148 (2010)
40. B. Hess, C. Holm, N. Vegt, J. Chem. Phys. **124**, 164509 (2006)
41. L. Perera, M.L. Berkowitz, J. Phys. Chem. **97**, 13803–13806 (1993)